

1 **Morphology and size of the particles emitted from a gasoline**
2 **direct injection-engine vehicle and their ageing in an**
3 **environmental chamber**

4
5 Jiaoping Xing^{a,b}, Longyi Shao^{a*}, Wenbin Zhang^c, Jianfei Peng^d, Wenhua wang^a, Shijin
6 Shuai^c, Min Hu^d, Daizhou Zhang^{e*}

7
8 ^aState Key Laboratory of Coal Resources and Safe Mining, School of Geoscience and Survey
9 Engineering, China University of Mining and Technology (Beijing), Beijing 100083, China.

10 ^b2011 Collaborative Innovation Center of Jiangxi Typical Trees Cultivation and Utilization, School of
11 Forestry, Jiangxi Agricultural University, Nanchang, 330045, China.

12 ^cState Key Laboratory of Automotive Safety and Energy, Department of Automotive Engineering,
13 Tsinghua University, Beijing 100084, China

14 ^dState Key Joint Laboratory of Environmental Simulation and Pollution Control, College of
15 Environmental Sciences and Engineering, Peking University, Beijing 100871, China

16 ^eFaculty of Environmental and Symbiotic Sciences, Prefectural University of Kumamoto, Kumamoto
17 862-8502, Japan

18
19 * Corresponding Author - e-mail: shaoL@cumtb.edu.cn (Longyi Shao); dzzhang@pu-kumamoto.ac.jp
20 (Daizhou Zhang)

21
22
23 **Highlights**

- 24 1. GDI-engine vehicles emitted a large amount of both primary and secondary organic
25 aerosols.
- 26 2. Higher contents of organic particles were emitted under hot stabilized running and
27 hot start states.
- 28 3. Sulfate and secondary organic aerosol formed on the surface of primary particles
29 after ageing.
- 30 4. Particles aged rapidly by catalyzed acidification under high pollution levels in
31 Beijing.

32
33
34

35 **Abstract:**

36 Air pollution is particularly severe in developing megacities, such as Beijing,
37 where vehicles equipped with modern gasoline direct injection (GDI) engines are
38 becoming one of major sources of the pollution. This study presents the characteristics
39 of individual particles emitted by a GDI gasoline vehicle and their ageing in a smog
40 chamber under the Beijing urban environment, as part of the Atmospheric Pollution &
41 Human Health (APHH) research programme. Using transmission electron microscopy,
42 we identified the particles emitted from a commercial GDI-engine vehicle running
43 under various conditions, namely, cold start, hot start, hot stabilized running, idle, and
44 acceleration states. Our results showed that most of the particles were organic, soot and
45 Ca-rich ones, with small quantities of S-rich and metal-containing particles. In terms of
46 particle size, the particles exhibited a bimodal distribution in number *vs* size, with one
47 mode at 800–900 nm, and the other at 140–240 nm. The amounts of organic particles
48 emitted under hot start and hot stabilized states were higher than those emitted under
49 other conditions. The amount of soot particles was higher under cold start and
50 acceleration states. Under the idle state, the proportion of Ca-rich particles was highest,
51 although their absolute number was low. In addition to quantifying the types of particles
52 emitted by the engine, we studied the ageing of the particles during 3.5 hours of
53 photochemical oxidation in an environmental chamber under the Beijing urban
54 environment. Ageing transformed soot particles into core-shell structures, coated by
55 secondary organic species, while the content of sulfur in Ca-rich and organic particles
56 increased. Overall, the majority of particles from GDI-engine vehicles were organic

57 and soot particles with submicron or nanometric size. The particles were highly reactive;
58 they reacted in the atmosphere and changed their morphology and composition within
59 hours via catalyzed acidification that involved gaseous pollutants at high pollution
60 levels in Beijing.

61

62 **1. Introduction**

63 Air pollution caused by PM_{2.5} in megacities such as Beijing, the capital city of
64 China, is of public and academic concerns due to its environmental impacts (Bond et
65 al., 2013; Huang et al., 2014; Liu et al., 2017) and adverse health effects (Chart-asa and
66 Gibson, 2015; Shao et al., 2017). Motor vehicle emissions are one of the most
67 significant sources of airborne particles in the urban atmosphere (Hwa and Yu, 2014),
68 and contribute up to 31% of primary particulate emissions of PM_{2.5} in Beijing (Yu et
69 al., 2013). Moreover, secondary aerosol formation associated with traffic emissions is
70 a major process leading to the rapid increase of PM_{2.5}, which results in severe haze
71 episodes (Huang et al., 2014). Although emissions from gasoline engines are relatively
72 lower than those from diesel engines (Alves et al., 2015), the number of gasoline-
73 powered vehicles in urban areas greatly exceeds that of diesel-powered vehicles. The
74 total number of vehicles in China reached 310 million in 2017, about 70% of these were
75 powered by gasoline engines (National Bureau of Statistics of China, 2018). There are
76 two main types of gasoline engines, namely, conventional multipoint port fuel injection
77 (PFI) engines and gasoline direct injection (GDI) engines. In recent years, the demand
78 for engines with high efficiency and low fuel consumption has led to an increasing use

79 of GDI engines in light-duty passenger cars. The market share of GDI-engine vehicles
80 has increased dramatically over the past decade and was estimated to reach 50% of new
81 gasoline vehicles sold in 2016 (Zimmerman et al., 2016). In Beijing and northern China,
82 the vehicle emissions become a more concerning issue in terms of air pollution when
83 the emission from coal combustion are seriously reduced after the Action for
84 Comprehensive Control of Air Pollution in Beijing since 2017 (Chang et al., 2019;
85 Chen et al. 2019; Zhang et al. 2019). In spite of this, regional transport of coal-burning
86 emissions from the surrounding areas can still influence the urban air sometimes
87 severely in winter (Ma et al., 2017; Zhang et al., 2019).

88 The number, mass and size distribution of particles emitted from GDI-engine
89 vehicles have been studied (Khalek et al., 2010; Maricq et al., 2011; Baral et al., 2011).
90 The size distribution usually has an accumulation mode with the maxima in the
91 diameter range of 100–300 nm. Major components of the particles include elemental
92 carbon (EC), organic carbon, and ash (Giechaskiel et al., 2014). Besides particulate
93 matter, the engines emit gaseous hydrocarbon compounds. These compounds might
94 form particles, or be adsorbed on the surface of particle aggregates, leading to the
95 growth of the particles in the engine emission (Luo et al., 2015). Relatively high particle
96 emissions by GDI-engine vehicles have prompted studies on the effects of engine
97 operating parameters and fuel composition on the characteristics of the particles (Hedge
98 et al., 2011; Szybist et al., 2011). It has been found that, in general, emissions under the
99 cold start condition make up the major contribution to the total amount of PM emissions
100 from GDI engines (Chen and Stone, 2011). Studies have also demonstrated that the

101 highest particle emissions from GDI engines in number concentration occur under the
102 acceleration state during transient vehicle operations (Chen et al., 2017).

103 Studies have also shown that gasoline vehicles are an important source of
104 secondary aerosol precursors in urban areas (Suarez-Bertoa et al., 2015). Secondary
105 aerosols can be formed via gas-phase reactions of volatile organic compounds and
106 multiphase and heterogeneous processes of primary particles (Zhu et al., 2017).
107 Experiments performed in environmental chambers demonstrated that the mass of
108 secondary aerosols derived from precursors could exceed that of directly-emitted
109 aerosols (Jathar et al., 2014). The occurrence of secondary aerosols on particles could
110 change the properties of particles in size, mass, chemical composition, morphology,
111 optical and hygroscopic parameters. These changes, in turn, might affect the
112 environmental impact of the particles significantly, for instance in terms of visibility,
113 human health, weather, and energy budgets (Laskin et al., 2015; Peng et al., 2017). In
114 general, the ageing processes of primary particles in the atmosphere are studied to
115 understand their climate effects (Niu et al., 2011). However, the lack of data on primary
116 particles emitted by gasoline engines hinders a deep understanding of the roles and
117 activities of the particles in ambient air pollution and relevant environmental effects.

118 Atmospheric Pollution & Human Health (APHH) research programme aimed to
119 explore the sources and processes affecting urban atmospheric pollution in Beijing.
120 Details regarding this project are given in Shi et al. (2018). To address one of the aims
121 of the AIRPOLL-Beijing (Source and Emissions of Air Pollutants) and AIRPRO-
122 Beijing (The integrated Study of AIR Pollution Processes), we employed a dedicated

123 experiment to investigate the characteristics of the individual particles, in terms of the
124 number concentration, size distribution, emitted from a GDI-engine vehicle during a
125 real-world driving cycle for chassis dynamometer test, i.e., the Beijing driving cycle
126 (BDC). Various test modes were introduced to accurately evaluate the emission from
127 light- or medium-duty vehicles. Furthermore, experiments were conducted in an
128 environmental chamber to investigate the ageing processes of particles emitted by GDI-
129 engine vehicles in ambient air in Beijing. We utilized a transmission electron
130 microscope equipped with an Oxford energy-dispersive X-ray spectrometer (TEM-
131 EDX) to identify the morphology, size and elemental composition of particles emitted
132 by the GDI-engine vehicle when it was running under different states. Particles before
133 and after a 3.5-hour ageing in the chamber were compared on the basis of the TEM-
134 EDX analysis. The TEM-EDX analysis provides the information on the internal
135 inhomogeneity, mixing state and surface characteristics of individual particles and has
136 been used to analyze the aerosol particles (Li and Shao, 2009; Loh et al., 2012; Adachi
137 and Buseck, 2015; Shao et al., 2017). The experimental design allows for the study of
138 the physical and chemical characteristics of the particles emitted from the GDI-engine
139 vehicles, as well as their ageing in a simulated urban atmosphere. The purposes of this
140 study are to evaluate the individual characteristics and the ageing process of primary
141 particles emitted by a GDI-engine vehicle, to investigate the ageing processes of such
142 particles in the atmosphere, and to deepen the understanding of the environmental
143 impact of gasoline-powered vehicle emissions.

144 **2. Material and methods**

145 **2.1 Test vehicle, fuels, and test procedure**

146 The GDI-engine vehicle utilized in the experiment complies with the China Phase
147 4 (equivalent to Euro 4) standard. It uses a three-way catalyst to reduce gaseous
148 emissions. The GDI (model GDI-1.4-T) in the test vehicle is recognized as a
149 representative of leading-edge designs of gasoline engines, because of its advanced
150 engine technologies such as its better fuel burning efficiency and lower greenhouse gas
151 emissions than other types of engine. Vehicles equipped with such GDI engines
152 constitute the majority of light-duty vehicles in China, especially in large cities like
153 Beijing. Details of the engine used in this study are listed in Table S1. The fuel used in
154 the experiment is a commercial gasoline blend of common quality in China. The
155 properties of the fuel were measured by SGS-CSTC Standards Technical Services Co.,
156 Ltd., China, and are listed in Table S2. The fuel has a Research Octane Number (RON)
157 of 93 and is a fifth-stage gasoline. It contains 36.7% of aromatics and 15.4% of olefins
158 in volume and has 6% of sulfur in mass, representing a typical fifth-stage gasoline in
159 China (with high aromatics) and is now widely used in Beijing. The experiments were
160 conducted within repeated Beijing Driving Cycles (BDCs), and one BCD included a
161 200-s “cold start” phase followed by an 867-s “hot stabilized running” phase. The
162 conditions during a BDC in the experiments are illustrated in Figure S1a. The cold start
163 state was achieved by starting the vehicle with a period of small accelerations, while
164 the hot stabilized running state had multiple periods of large acceleration and a
165 maximum velocity of 50 km h⁻¹. The BDC, characterized by a higher proportion of
166 idling periods and a lower acceleration speed than the New European Driving Cycle

167 (NEDC), was performed to simulate the repeated braking and acceleration on road in
168 megacities such as Beijing.

169 All tests were performed on a Euro 5/LEV2/Tier 2-capable test cell on a 48-inch
170 single-roll chassis dynamometer at the State Key Laboratory of Automobile Safety and
171 Energy Conservation at Tsinghua University. The test procedure for each run was as
172 follows: fuel change, BDC preparation, soak, cold start BDC test, and hot start BDC
173 test. After fuel change and BDC preparation, the test vehicle was then conditioned with
174 an overnight soak for more than 10 h. The soak room temperature was maintained
175 between 20 and 30 °C. Due to the limitation of the facilities and available running time,
176 a hot start test was conducted within 5 mins after the cold start test. A dilution unit was
177 applied to dilute the exhaust from the tailpipe into 1/10 in volume using synthetic air
178 composed of 79% N₂ and 20% O₂, in order to obtain the concentrations suitable for
179 subsequent measurements and suppress possible coagulation. The number
180 concentration of the emitted particles was monitored by a Combustion Fast Particle
181 Size Spectrometer Differential Mobility Spectrometer 500 (DMS 500). The maximum
182 measurable number concentration of DMS 500 was 10¹¹ (dN/dlogDp/cc) after the
183 dilution (Petzold et al., 2011). For the analyses of individual particles, 6–8 samples
184 were collected during one BDC test. At least one sample was collected under each
185 running state (i.e. cold start, hot start, idle state, acceleration state, or hot stabilized
186 running state). The driving cycle test was repeated at least twice. Two or more samples
187 were obtained for each running state. A single-stage cascade impactor (KB-2, Qingdao
188 Jinshida Company) was mounted to the exit of the tailpipe after the dilution unit. The

189 emitted particles were collected onto 300-mesh copper TEM grids, which were covered
190 with a carbon-coated formvar film. The flow rate was 1.0 L min^{-1} , and the cut-off
191 diameter of the impactor for 50% collection efficiency was $0.25 \text{ }\mu\text{m}$ if the density of
192 the particles was 2 g cm^{-3} . For each sample, the collection time was 60 s.

193 **2.2 Environmental chamber experiments**

194 Particles from the GDI-engine vehicle were introduced into an environmental
195 chamber and exposed to sunlight. The chamber, made of perfluoroalkoxy (PFA) Teflon
196 in order to achieve a high transmission of ultraviolet light, has an internal volume of
197 1.2 m^3 . Ambient sunlight was used as the driving force for photochemical reactions in
198 the chamber, in an environment close to actual open air. Before the experiments, the
199 chamber was cleaned by flushing with zero air for approximately 12 hours and
200 illuminated with sunlight, to remove residues that could influence the experiments.
201 H_2O_2 (1 mL, 30%), together with the vehicle emission, was injected into the chamber
202 to generate OH exposure. The OH exposure at the end of the experiments reproduced
203 extreme oxidation processes, which were equivalent to cases of an oxidation more than
204 10 days in Beijing ambient air if the 24-hour-mean concentration of OH is 10^6
205 molecules cm^{-3} (Lu et al., 2013). The aging experiments for the gasoline exhausts were
206 carried out with a relatively high OH exposure compared to ambient conditions in order
207 to obtain the aging process. This method and the amount of H_2O_2 have been frequently
208 used in smog chamber experiments (Song et al., 2007; Song et al., 2019). After the
209 injection, the experiments were conducted from approximately 13:00 to 17:00 local
210 time under sunshine, with the relative humidity being kept at around 50%. The global
211 solar radiation when the tests were carried out was approximately 318 W m^{-2} . After 3.5

212 h of ageing, the particles in the chamber were collected onto mesh TEM grids using the
213 impactor. The collection time for each sample was 120 s. The schematic diagram of the
214 experimental system is presented in Figure S1b.

215

216 **2.3 TEM/EDX and scanning transmission electron microscopy (STEM) analyses**

217 The particles in the samples were examined using a Tecnai G2 F30 field emission
218 high-resolution transmission electron microscope (FE-HRTEM). This microscope is
219 also equipped with an Oxford EDX and a STEM unit with a high-angle annular dark-
220 field detector (HAADF). The EDX can detect elements with the atom number larger
221 than 5 (B) in a single particle. The HAADF can detect the distribution of a certain
222 element by mapping the distribution of the element in a particle. The TEM was operated
223 with the acceleration voltage of 300 kV. EDX spectra were firstly collected for 20 live
224 seconds to minimize the influence of radiation exposure and potential beam damage
225 and then for 90 live seconds for a range of possible elements. Copper was excluded
226 from the analysis because of interference from the TEM grids which were made of
227 copper.

228 To ensure the representativeness of the analyzed particles, more than 150 particles
229 from at least 3 random areas were analyzed from the center and periphery of the
230 sampling spot on each grid. All individual particles larger than 50 nm in the selected
231 areas were analyzed. The TEM images were digitized using an automated fringe image
232 processing system named Microscopic Particle Size of Digital Image Analysis System
233 (UK) to project the surface areas of the particles. The equivalent spherical diameter of
234 a particle was calculated from its projected area, expressed as the square root of $4A/\pi$,

235 where A was the projected area. The electron microscope analysis of individual particles
236 was very time consuming, which hindered us from analyzing more particles from
237 multiple engines emission. There are differences in emissions from vehicles to vehicles,
238 even for vehicles with same model engines. Only one GDI vehicle, the type of which
239 constitutes the majority of light-duty vehicles in China, was tested in this study. The
240 representativeness of the present results remains unevaluated carefully with, such as,
241 comparisons between vehicles to achieve broader statistical results, although the tests
242 in the present studies were conducted under strict control conditions.

243 **3. Results**

244 **3.1. Particle morphology, elemental composition and size**

245 A total of 2880 particles were analyzed from the GDI-engine vehicles. Most of the
246 particles were in the sub-micrometer size range. Based on morphology and elemental
247 composition of the particles, the majority of them were identified as soot, organic and
248 Ca-rich particles, a smaller amount was identified as S-rich or metal-rich particles (Fig.
249 1). The method of particle classification is similar to that adopted by Okada et al. (2005)
250 and Xing et al. (2019). In the following description, “X-rich” means that the element
251 “X” occupies the largest proportion in the element composition of the particles. Figure
252 2 illustrates the number-size distributions of the relative concentration ($dN/d\log D$) of
253 primary particles from the GDI-engine vehicle, where N is the relative number fraction
254 and D is the equivalent diameter. The particles were in the range of 60–2500 nm and
255 displayed a bimodal distribution, with one mode in the 140–240 nm range, and another
256 in the 800–900 nm range. Particles smaller than 250 nm were largely underestimated
257 because of the loss during the particle collection. Therefore, there should have been

258 more particles in the smaller mode range than shown in Figure 2. Concerning the loss
259 of small particles, we measured the size distribution by the DMS500 (Fig. S2). The
260 results showed that a large amount of nucleation mode particles were emitted by the
261 GDI vehicle.

262 It should be noted that organic particles were mainly composed of C and O
263 elements, and contained a small amount of inorganic elements Ca, P, S and Zn.
264 Elemental mapping of the organic particles exhibited the presence of Ca, P, S and Zn in
265 some of the particles, showing the mixture state of organic and inorganic materials (Fig.
266 1f). It has been reported that such particles could be related to the combustion of fuels
267 or lubrication oil (Rönkkö et al., 2013). In addition to these primary organic particles,
268 the GDI-engine vehicle emitted precursor gases, which produced secondary organic
269 particles via gas-phase reactions, and multiphase and heterogeneous processes on the
270 primary particles. A group of spherical particles were found in the environmental
271 chamber (Fig. 1g). These particles became semi-transparent or transparent to an
272 electron beam, which was characteristic of organic materials, liquid water, or their
273 evaporation residues either mixed or not mixed with electron absorptive materials. We
274 regarded these particles as secondary organic particles because the humidity in the
275 chamber during the experiment was kept much below saturation (relative humidity
276 around 50%). Therefore, these particles were expected to mainly consist of secondary
277 organic materials, which should have been produced via gas phase reactions or on the
278 surface of pre-existing particles (Hu et al., 2016). No other elements, except C and O,
279 were identified in these particles, which was consistent with the above inference.

280 Similar particles were also encountered in other environmental chamber experiments
281 studying emissions from light-duty gasoline vehicles (Jathar et al., 2014).

282

283 **3.2 Number fractions of particles**

284 Figure 3 illustrates the numbers of accumulation mode particles emitted by
285 burning one kilogram of fuel during the cold start and hot start driving cycles. PM
286 emissions at the start-up stage under both cold and hot start states were higher than the
287 emissions under the states when the engine was fully warmed and the vehicle operation
288 was stabilized. The PM emission was the highest under the hot stabilized running state
289 (2.3×10^{10} particles (kg fuel)⁻¹), followed by those under the hot start (1.2×10^{10} particles
290 (kg fuel)⁻¹), cold start (7.1×10^9 particles (kg fuel)⁻¹), and acceleration running states
291 (2.9×10^9 particles (kg fuel)⁻¹), with the emission under the idle running state being the
292 lowest (7.4×10^8 particles (kg fuel)⁻¹) (Fig. S3). The higher emission of particle in term
293 of number for the GDI vehicle under the hot start state can be ascribed to the
294 experimental time of the vehicle engine. The hot start test in this study was conducted
295 within 5 mins after the cold start test. The PM emissions from GDI vehicles were
296 relatively less affected by ambient temperature for the initial 30 minutes during the
297 warming up of the engines (Cotte et al., 2001). This may lead to the high value of the
298 PM emission for the hot start state which is slightly higher than that for the cold start
299 state. Although the total PM emission were higher under hot start state than that under
300 the cold start state, the comparison of those in the size range of accumulation mode
301 indicates that the particulate emissions for this mode of particles were higher under the
302 cold start state than under the hot start sate (Fig. 3). This can be attributed to the less

303 efficiency of the vaporization of fuel droplets in the combustion cylinder under the cold
304 start state (Chen et al., 2017). Size distributions of the particles varied with driving
305 conditions (Fig. S4). Under the cold start state and acceleration running state, higher
306 number concentrations, and thus higher mass concentrations of the particles with
307 accumulation mode were emitted in comparison with other running states.

308 Under all the running states, morphologies and types of the particles remained
309 similar but the proportions of different types of particles differed considerably (Fig. S5).
310 The proportion of organic particles was high under hot stabilized and hot start states.
311 Soot particles were abundant under cold start and acceleration states. A relatively higher
312 proportion of Ca-rich particles was found under idle state, compared to those under
313 other running states.

314 We estimated the number of different type particles in the emission under the
315 running states by burning one kilogram of fuel (Fig. 4). Organic particles in the
316 emission under the hot stabilized running state (2.3×10^9 particles (kg fuel)⁻¹) and the
317 hot start running state (3.6×10^8 particles (kg fuel)⁻¹) were higher than in the emission
318 under other running states. The number of soot particles were higher under the hot
319 stabilized running state (1.7×10^9 particles (kg fuel)⁻¹) and the cold start state (5.9×10^8
320 particles (kg fuel)⁻¹) than those under other running states. Under the idle state, the
321 relative proportion of Ca-rich particles was the highest, although their absolute number
322 was low (1.4×10^9 particles (kg fuel)⁻¹).

323 Under the cold start state, a significant proportion of the emitted particles were
324 soot particles. This can be attributed to the incomplete vaporization of fuel droplets in

325 the combustion cylinder (Chen et al., 2017). Under the hot start state and the hot
326 stabilized running state, organic particles were predominant. Under these two running
327 states, the engine temperature was high, which enabled the fuel to evaporate and mix
328 with the air easily. With the increase of the temperature in the cylinders, the rate of
329 particle oxidation increased, which could cause an increase of organic particles in the
330 emission (Fu et al., 2014). Under the idle state, the fuel consumption was much lower
331 than that under the other running states, which resulted in a higher relative contribution
332 to particles from lubricant oil. The high Ca content in the lubricant oil led to a higher
333 Ca-rich particle emission under this running state. Under the acceleration state, the
334 predominant types of particle included soot, organic, and Ca-rich particles. As the
335 acceleration running required a high vehicular speed and engine load, the emissions
336 contained more soot particles than those under other running states.

337 **3.3. Aged particles in the environmental chamber**

338 A large amount of secondary organic particles (accounting for 80%-85% in
339 number), some soot particles, Ca-rich particles, and primary organic particles were
340 detected in the environmental chamber (Fig. 5). After the ageing process, many soot
341 particles changed into core-shell structures and became coated with secondary species
342 (Figs. 5b and 5c). The EDX results showed that almost all coatings were mainly
343 composed of C, O, and S, suggesting these coatings were a mixture of organic and
344 sulfate. The morphology and compositions of Ca-rich particles and organic particles
345 (Figs. 5e and 5g) changed, with the aged ones having a more irregular shape and a
346 higher sulfur content in comparison with fresh ones (Figs. 5A and B).

347 Approximately 80% of the soot particles were present in core-shell structures and

348 coated with secondary species after the 3.5-hour ageing. In contrast, before the ageing,
349 the particles with a core-shell structure were only about 10% of the total. The mean
350 diameter of the soot particles after ageing was around 0.49 μm , which was much smaller
351 than that before the ageing (0.65 μm), indicating the shrinkage of the soot particles
352 during the ageing (Fig. 5b). The core-shell ratios, defined as the ratio of the diameter of
353 the core part (D_{core}) to the diameter of the whole particle (D_{shell}) (Niu et al., 2016;
354 Hou et al., 2018), were used to quantify the aging degree of the soot particles with
355 coating. It was found that the core-shell ratios of the soot particles in the smog chamber
356 were mainly in the range of 0.25–0.78, indicating the stronger aging degree of soot
357 particles in the chamber than case data in urban air with the ratios of 0.4–0.9 (Niu et al.,
358 2016).”

359 **4. Discussion**

360 **4.1. Contribution of GDI-engine vehicle emissions to urban air pollution**

361 Our investigation showed that the GDI-engine vehicle emitted a large amount of
362 organic particles (32%), soot (32%), Ca-rich particles (26%), S-rich (5%) and metal-
363 containing particles (4%). Relevant studies have also shown that the primary
364 carbonaceous aerosols (element carbon + primary organic aerosol) accounted for 85 %
365 of the PM in the GDI vehicles, suggesting that carbonaceous aerosols were the major
366 contributors in the PM from GDI gasoline vehicles (Du et al., 2018). Considering the
367 large fraction of the vehicles equipped with GDI engines in megacities like Beijing, this
368 indicates a possible substantial contribution of GDI-engine vehicles to urban air
369 pollution. Moreover, organic particles occupied the majority of the particles emitted

370 under hot stabilized running and hot start states. It has been noted that the organic matter
371 was the major component of the total particle mass during the hot start conditions
372 (Fushimi et al., 2016; Chen et al., 2017), which was consistent with the results obtained
373 for the number concentrations in our study. The hot stabilized running state is the most
374 frequent running condition of vehicles, whereas the hot start state is the most frequent
375 condition in congested traffic. This suggests that a substantial number of organic
376 compounds in the air pollution of populated cities might be directly related to vehicle
377 emissions.

378 Organic particles and soot particles in ambient air are emitted from a range of
379 sources including fossil fuels, biomass burning and urban waste burning (Kanakidou et
380 al., 2005). Table 1 shows the major characteristics of particles in the emissions from
381 different sources. For instance, there is a higher fraction of soot particles and a lower
382 fraction of organic particles in the emissions of GDI-engine vehicles compared to PFI-
383 engine vehicles (Xing et al., 2017). Organic particles in emissions from gasoline
384 vehicles are usually enriched in Ca, S and P (Xing et al., 2017; Liati et al., 2018). In
385 comparison, emissions from biomass/wood burning are usually dominated by organic
386 particles, which account for more than 50% of the total amount of particles (Liu et al.,
387 2017). Furthermore, organic particles from biomass/wood burning usually show
388 elevated K content, and thus, this element is frequently used as an indicator for
389 biomass/wood burning organic particles (Niu et al., 2016). Observations of primary
390 particles directly from coal burning have also demonstrated a predominance of organic
391 particles, soot particles, S-rich particles and mineral particles (Zhang et al., 2018; Wang

392 et al., 2019). Both biomass burning and coal combustion can produce organic particles
393 and almost all the emitted particles contain a certain amount of Si in addition to C and
394 O. Table 1 also shows the elemental concentrations in the organic particles in the
395 emissions from different types of sources. Since the concentrations of minor elements
396 in the organic particles are highly dependent on the sources, they could be used for
397 source identification of individual particles in the atmosphere.

398 The present data also permit the compilation of a rough inventory of particle
399 categories and amounts emitted from GDI-engine vehicles under various running
400 conditions (Fig. 4). Combined with statistics on the number of vehicles with GDI
401 engines, the running time and the running conditions on roads within a certain area, it
402 is possible to make an approximate estimate of the amounts of primary particles emitted
403 from GDI-engine vehicles. Such estimate is the basis for accurate source apportionment
404 of particles from vehicles, and it will be very beneficial for studies on the anthropogenic
405 sources of primary particles in urban air. These data could be brought together to better
406 understand the sources of air pollutants in the Beijing megacity and to improve the
407 capability of developing cost-effective mitigation measures.

408 **4.2 Rapid ageing of primary particles in Beijing**

409 The results of chamber experiments indicate that sulfate and secondary organic
410 aerosol (SOA) form on the surface of soot, Ca-rich and organic particles. Moreover, the
411 atmospheric transformation of primary particles emitted by the GDI-engine vehicles
412 could occur within 3.5 hours, indicating the ageing was rapid. Peng et al. (2014) found
413 similar timescales for black carbon transformation under polluted conditions in Beijing.

414 The rapid ageing of primary particles could be caused by several factors, such as the
415 concentration of gaseous pollutants from the vehicles, strength of solar radiation,
416 relative humidity (RH), and O₃ concentration (Guo et al., 2012; Deng et al., 2017; Du
417 et al., 2018). The present experiments were conducted in the atmosphere with relative
418 humidity of approximately 50% and solar radiation of 318 Wm⁻². The total hydrocarbon
419 emission (THC) from the GDI vehicles was 0.297 g km⁻¹. Repeated braking and
420 acceleration in the BDC could cause incomplete combustion and consequently high
421 THC emission. Under a high concentration of gaseous pollutants, primary particles
422 would age rapidly when exposed to solar radiation. Consequently, secondary species
423 including SOA and sulfate were produced on or condensed onto the particles, leading
424 to the coating. Guo et al. (2014) also showed that secondary photochemical growth of
425 fine aerosols during the initial stage of haze development could be attributed to highly
426 elevated levels of gaseous pollutants.

427 The mixture of SOA and sulfate have been detected in our chamber experiment,
428 indicating the involvement of inorganic salts in the SOA formation. Previous studies
429 have demonstrated the enhancement of SOA production in the presence of inorganic
430 sulfate (Beardsley and Jang, 2015; Kuwata et al., 2015), and this is because sulfate can
431 catalyze carbonyl heterogeneous reactions, and consequently, lead to SOA production
432 (Jang et al., 2002; Jang et al., 2004). Moreover, these aged primary particles favored
433 the formation of secondary aerosols by providing reaction sites and reaction catalysts.
434 Sulfate and secondary organic aerosol (SOA) co-existed on the surface of primary
435 particles, such as soot, Ca-rich and organic particles. In addition, the products of VOCs

436 oxidation could react with SO₂ to rapidly produce sulfate (Mauldin et al., 2012). Thus,
437 the rapid ageing of primary particles could also be attributable to the acid-catalyzed
438 mechanism. As the major source of pollutants in urban air, the GDI-engine vehicles
439 supply both primary particles and precursor gaseous species, and the rapid ageing of
440 the particles under certain conditions is very likely to be the major driving force for the
441 elevation of urban air pollution.

442 **4.3 Implications and perspectives**

443 Our results indicated that GDI-engine vehicles emitted a large amount of both
444 primary and secondary organic aerosols. PM number emission of organic particles from
445 GDI-engine vehicle were 2.9×10^9 particles (kg fuel)⁻¹ during the BDC. Secondary
446 organic particle was predominant in the secondary aerosols, accounting for 80-85%%
447 particles in the chamber. Organic aerosols (OA) play an important role in the Earth's
448 radiation balance not only for its absorption and scattering of solar radiation but also
449 because they can alter the microphysical properties of clouds (Scott et al., 2014).
450 Particle size, shape, mixing state and composition affect their light scatterings and
451 absorption cross sections, and cloud condensation nuclei activity (Jacobson, 2001). OA
452 are composed of various types of chemical compounds with varying absorption
453 properties (mixing state), which are determined by the emission sources, the formation
454 mechanism (Zhu et al., 2017), and the source regions (Laskin et al., 2015). Primary OA
455 from biomass burning is co-emitted with soot (black carbon), inorganic salts, and fly
456 ash, producing internally and externally mixed particles in which the organic
457 components are present in different relative abundance (Lack et al., 2012). Similarity,

458 primary OA in the exhaust of gasoline and diesel vehicles are mixed with Ca, P, Mg,
459 Zn, Fe, S, and minor Sn inorganic compounds (Liati et al., 2018). In addition, previous
460 measurements have indicated that SOA usually exists as an internal mixture with other
461 aerosols, such as sulfate, ammonium, or nitrate (Zhu et al., 2017). Our results showed
462 that the POA emitted from GDI-engine vehicle were mixed with soot, inorganic
463 components such as Ca, P, and Zn. Some of the SOA formed in the smog chamber were
464 mixed with sulfate. The complexity of mixing state makes it difficult to characterize the
465 properties of OA. Lang-Yona et al. (2010) have found that for aerosols consisting of a
466 strongly absorbing core coated by a non-absorbing shell, the Mie theory prediction
467 deviate from the measurements by up to 10%. Moreover, atmospheric aging process,
468 involving aqueous-phase aging and atmospheric oxidation, can either enhance or
469 reduce light absorption by OA (Bones et al., 2010). The condensation process may
470 result in a dramatic enhancement of hydrolysis of OA compounds, affecting their
471 absorption spectra (Lambe et al., 2015).

472 Our results also showed that primary organic aerosols (POA) emitted by GDI-
473 engine vehicles could acquire OA and sulfate coatings rapidly, within a few hours, and
474 increase a sizable fraction of total ambient aerosols existing as internal mixtures. In
475 addition, the fast ageing further caused the increase of aged POA in the total OA,
476 consequently, largely modified the properties of the particles such as their optical
477 properties. The results of the experiments in the chamber showed that most of the aged
478 POA had a core-shell structure, whereas most of the secondary organic aerosols (SOA)
479 produced by gas-phase reactions had a uniform structure. These results push forward

480 the understanding on the mixing state and chemical composition of both POA and SOA.
481 The experimental data will benefit the parameterization of vehicles emissions in
482 numerical models dealing with urban air pollution.

483 **5. Conclusions**

484

485 1. Five types of individual particles emitted by a GDI-engine gasoline vehicle were
486 identified, including soot, organic, Ca-rich, S-rich, and metal-rich particles. Among
487 them, soot, organic, and Ca-rich particles were predominant. The particles emitted
488 from this commercial GDI-engine gasoline vehicle displayed a bimodal size
489 distribution.

490 2. The concentrations of the particles emitted by this commercial GDI-engine
491 gasoline vehicle vary with different running conditions. The PM emission was the
492 highest under the hot stabilized running state, followed by those under the hot start,
493 cold start, and acceleration running states, with the emission under the idle running
494 state being the lowest under the idle running state.

495 3. The relative proportions of the different types of particles emitted by this
496 commercial GDI-engine gasoline vehicle varied with different running conditions.
497 Large amounts of organic particles were emitted during hot stabilized and hot start
498 states. Under cold start and acceleration states, the emissions were enriched in soot
499 particles. Under idle state, a relatively higher number of Ca-rich particles was
500 emitted, although the absolute number was low.

501 4. After ageing in the environmental chamber, the structure of the soot particles
502 changed into a core-shell structure, and the particles were coated with condensed

503 secondary organic material. Ca-rich particles and organic particles also were
504 modified, and their content of sulfur increased after ageing.

505 5. Ageing of the emitted particles occurred rapidly, within hours. Such rapid ageing
506 could be attributable to an acid-catalyzed mechanism and to the high initial
507 concentrations of gaseous pollutants emitted by this commercial GDI-engine
508 gasoline vehicle.

509

510 **Data availability**

511 All data presented in this paper are available upon request. Please contact the
512 corresponding author (shaoL@cumtb.edu.cn).

513 **Author contribution**

514 LS designed this study; JX performed the experiments. JX, LS, DZ summarized
515 the data and wrote the paper. WZ, JP, WW, SS, MH supported the experiments and
516 commented the paper.

517 **Competing interests**

518 The authors declare that they have no conflict of interest.

519 **Acknowledgements**

520 This work was supported by Projects of International Cooperation and Exchanges
521 NSFC (Grant No. 41571130031). The data analysis was partly supported by Science
522 and Technology Project Founded by the Education Department of Jiangxi Province (No.
523 GJJ180226), Yue Qi Scholar Fund of China University of Mining and Technology
524 (Beijing), and a Grant-in-Aid for Scientific Research (B) (No.16H02942) from the

525 JSPS.

526 **References**

- 527 Adachi, K., and Buseck, P. R.: Changes in shape and composition of sea-salt particles upon aging in an
528 urban atmosphere, *Atmos. Environ.*, 100, 1-9, <http://dio.org/10.1016/j.atmosenv.2014.10.036>, 2015.
- 529 Alves, C. A., Lopes, D. J., Calvo, A. I., Evtyugina, M., Rocha, S., and Nunes, T.: Emissions from light-
530 duty diesel and gasoline in-use vehicles measured on chassis dynamometer test cycles, *Aerosol Air*
531 *Qual. Res.*, 15(1), 99-116, <http://dio.org/10.4209/aaqr.2014.01.0006>, 2015.
- 532 Baral, B., Raine, R., and Miskelly, G.: Effect of engine operating conditions on spark-ignition engine
533 PAH emissions, *SAE Technical Paper 2011-01-1161*, <http://dio.org/10.4271/2011-01-1161>, 2011.
- 534 Beardsley, R.L., and Jang, M.: Simulating the SOA formation of isoprene from partitioning and
535 aerosol phase reactions in the presence of inorganics, *Atmos Chem Phys*, 15, 33121-33159,
536 <http://dio.org/10.5194/acpd-15-33121-2015>, 2015.
- 537 Bond, T. C., Doherty, S. J., Fahey, D. W., Forster, P. M., Berntsen, T., DeAngelo, B. J., Flanner, M. G.,
538 Ghan, S., Kärcher, B., Koch, D., Kinne, S., Kondo, Y., Quinn, P. K., Sarofim, M. C., Schultz, M.
539 G., Schulz, M., Venkataraman, C., Zhang, H., Zhang, S., Bellouin, N., Guttikunda, S. K., Hopke, P.
540 K., Jacobson, M. Z., Kaiser, J. W., Klimont, Z., Lohmann, U., Schwarz, J. P., Shindell, D.,
541 Storelvmo, T., Warren, S. G., and Zender, C. S.: Bounding the role of black carbon in the climate
542 system: A scientific assessment, *J. Geophys. Res.-Atmos.*, 118(11), 5380-5552,
543 <http://dio.org/10.1002/jgrd.50171>, 2013.
- 544 Bones, D.L., Henricksen, D.K., Mang, S.A., Gonsior, M., Bateman, A.P., Nguyen, T.B., Cooper,
545 W.J., and Nizkorodov, S.A.: Appearance of strong absorbers and fluorophores in limonene-O₃
546 secondary organic aerosol due to NH⁴⁺-mediated chemical aging over long time scales, *J*
547 *Geophys Res*, 115, <http://dio.org/10.1029/2009JD012864>, 2010.
- 548 Chart-asa, C., and Gibson, J. M.: Health impact assessment of traffic-related air pollution at the urban project scale: Influence of
549 variability and uncertainty, *Sci. Total Environ.*, 506-507, 409-421,
550 <http://dio.org/10.1016/j.scitotenv.2014.11.020>, 2015.
- 551 Chang, L., Shao, L., Yang, S., Li, J., Zhang, M., Feng, X., Li, Y., 2019, Study on variation characteristics
552 of PM_{2.5} mass concentrations in Beijing after the action for comprehensive control of air pollution.
553 *Journal of Mining Science and Technology*, 2019, 4(6): 539-546. <http://dio.org/10.19606/j.cnki.jmst.2019.06.009>. (in Chinese with English Abstract)
- 554 Chart-asa, C., and Gibson, J. M.: Health impact assessment of traffic-related air pollution at the urban
555 project scale: Influence of variability and uncertainty, *Sci. Total Environ.*, 506-507, 409-421,
556 <http://dio.org/10.1016/j.scitotenv.2014.11.020>, 2015.
- 557 Chen, Z., Chen, D., Xie, X., Cai, J., Zhuang, Y., Cheng, N., He, B., and Gao, B.: Spatial self-aggregation
558 effects and national division of city-level PM_{2.5} concentrations in China based on spatio-temporal
559 clustering, *J. Clean. Prod.*, 207, 875-881, <http://dio.org/10.1016/j.jclepro.2018.10.080>, 2019.
- 560 Chen, L., Liang, Z., Zhang, X., and Shuai, S.: Characterizing particulate matter emissions from GDI and
561 PFI vehicles under transient and cold start conditions, *Fuel*, 189, 131-140,
562 <http://dio.org/10.1016/j.fuel.2016.10.055>, 2017.
- 563 Chen, L., and Stone, R.: Measurement of enthalpies of vaporization of isooctane and ethanol blends and
564 their effects on PM emissions from a GDI engine, *Energ. Fuel*, 25(3), 1254-1259,
565 <http://dio.org/10.1021/ef1015796>, 2011.
- 566

567 Cotte, H., Bessagnet, B., Blondeau, C., Mallet-Hubert, P.Y., Momique, J.C., Walter, C., Boulanger, L.,
568 Deleger, D., Jouvenot, G., Pain, C., and Rouveïrolles, P.: Cold-start emissions from petrol and diesel
569 vehicles according to the emissions regulations (from Euro 92 to Euro 2000), *Int J Vehicle Des*, 27,
570 275-285, 10.1504/IJVD.2001.001971, 2001.

571 Deng, W., Hu, Q., Liu, T., Wang, X., Zhang, Y., Song, W., Sun, Y., Bi, X., Yu, J., Yang, W., Huang, X.,
572 Zhang, Z., Huang, Z., He, Q., Mellouki, A., and George, C.: Primary particulate emissions and
573 secondary organic aerosol (SOA) formation from idling diesel vehicle exhaust in China, *Sci. Total*
574 *Environ.*, 593-594, 462-469, <http://dio.org/10.1016/j.scitotenv.2017.03.088>, 2017.

575 Du, Z., Hu, M., Peng, J., Zhang, W., Zheng, J., Gu, F., Qin, Y., Yang, Y., Li, M., Wu, Y., Shao, M., and
576 Shuai, S.: Comparison of primary aerosol emission and secondary aerosol formation from gasoline
577 direct injection and port fuel injection vehicles, *Atmos. Chem. Phys.*, 18(12), 9011-9023,
578 <http://dio.org/10.5194/acp-18-9011-2018>, 2018.

579 Fu, H., Wang, Y., Li, X., and Shuai, S.: Impacts of cold-start and gasoline RON on particulate emission
580 from vehicles powered by GDI and PFI engines, *SAE Technical Paper 2014-01-2836*, [http://dio.org/](http://dio.org/10.4271/2014-01-2836)
581 [10.4271/2014-01-2836](http://dio.org/10.4271/2014-01-2836), 2014.

582 Fushimi, A., Kondo, Y., Kobayashi, S., Fujitani, Y., Saitoh, K., Takami, A., and Tanabe, K.:
583 Chemical composition and source of fine and nanoparticles from recent direct injection
584 gasoline passenger cars: Effects of fuel and ambient temperature, *Atmos Environ*, 124, 77-84,
585 <http://dio.org/10.1016/j.atmosenv.2015.11.017>, 2016.

586 Giechaskiel, B., Maricq, M., Ntziachristos, L., Dardiotis, C., Wang, X., Axmann, H., Bergmann, A., and
587 Schindler, W.: Review of motor vehicle particulate emissions sampling and measurement: From
588 smoke and filter mass to particle number, *J. Aerosol Sci.*, 67, 48-86,
589 <http://dio.org/10.1016/j.jaerosci.2013.09.003>, 2014.

590 Guo, S., Hu, M., Guo, Q., Zhang, X., Zheng, M., Zheng, J., Chang, C. C., Schauer, J. J., and Zhang, R.:
591 Primary sources and secondary formation of organic aerosols in Beijing, China, *Environ. Sci.*
592 *Technol.*, 18(46), 9846 - 9853, 2012.

593 Hedge, M., Weber, P., Gingrich, J., Alger, T., and Khalek, I. A.: Effect of EGR on Particle Emissions
594 from a GDI Engine, *SAE Int. J. Engines*, 4(1), 650- 666, <http://dio.org/10.4271/2011-01-0636>, 2011.

595 Hou, C., Shao, L., Hu, W., Zhang, D., Zhao, C., Xing, J., Huang, X., and Hu, M.: Characteristics
596 and aging of traffic-derived particles in a highway tunnel at a coastal city in southern China,
597 *Sci Total Environ*, 619-620, 1385-1393, <http://dio.org/10.1016/j.scitotenv.2017.11.165>, 2018.

598 Hu, W., Niu, H., Zhang, D., Wu, Z., Chen, C., Wu, Y., Shang, D., and Hu, M.: Insights into a dust event
599 transported through Beijing in spring 2012: Morphology, chemical composition and impact on
600 surface aerosols, *Sci. Total Environ.*, 565, 287-298, <http://dio.org/10.1016/j.scitotenv.2016.04.175>,
601 2016.

602 Huang, R., Zhang, Y., Bozzetti, C., Ho, K., Cao, J., Han, Y., Daellenbach, K. R., Slowik, J. G., Platt, S.
603 M., Canonaco, F., Zotter, P., Wolf, R., Pieber, S. M., Bruns, E. A., Crippa, M., Ciarelli, G.,
604 Piazzalunga, A., Schwikowski, M., Abbazade, G., Schnelle-Kreis, J., Zimmermann, R., An, Z.,
605 Szidat, S., Baltensperger, U., Haddad, I. E., and Prévôt, A. S. H.: High secondary aerosol
606 contribution to particulate pollution during haze events in China, *Nature*, 514(7521), 218-222,
607 <http://dio.org/10.1038/nature13774>, 2014.

608 Hwa, M., and Yu, T.: Development of real-world driving cycles and estimation of emission factors
609 for in-use light-duty gasoline vehicles in urban areas, *Environ Monit Assess*, 186, 3985-3994,
610 <http://dio.org/10.1007/s10661-014-3673-1>, 2014.

611 Jacobson, M. Z.: Strong radiative heating due to the mixing state of black carbon in atmospheric aerosols,
612 Nature, 409(6821), 695-697, <http://dio.org/10.1038/35055518>, 2001.

613 Jang, M. S., Czoschke, N. M., Lee, S., and Kamens, R. M.: Heterogeneous atmospheric aerosol
614 production by acid-catalyzed particle-phase reactions, Science, 298(5594), 814-817,
615 <http://dio.org/10.1126/science.1075798>, 2002.

616 Jang, M., Czoschke, N. M., and Northcross, A. L.: Atmospheric organic aerosol production by
617 heterogeneous acid-catalyzed reactions, Chemphyschem, 5(11), 1647-1661,
618 <http://dio.org/10.1002/cphc.200301077>, 2004.

619 Jathar, S. H., Gordon, T. D., Hennigan, C. J., Pye, H. O. T., Pouliot, G., Adams, P. J., Donahue, N. M.,
620 and Robinson, A. L.: Unspeciated organic emissions from combustion sources and their influence
621 on the secondary organic aerosol budget in the United States, P. Natl. Acad. Sci. USA, 111(29),
622 10473-10478, <http://dio.org/10.1073/pnas.1323740111>, 2014.

623 Kanakidou, M., Seinfeld, J. H., Pandis, S. N., Barnes, I., Dentener, F. J., Facchini, M. C., Van Dingenen,
624 R., Ervens, B., Nenes, A., Nielsen, C. J., Swietlicki, E., Putaud, J. P., Balkanski, Y., Fuzzi, S., Horth,
625 J., Moortgat, G. K., Winterhalter, R., Myhre, C., Tsigaridis, K., Vignati, E., Stephanou, E. G., and
626 Wilson, J.: Organic aerosol and global climate modelling: A review, Atmos. Chem. Phys., 5, 1053-
627 1123, <http://dio.org/10.5194/acp-5-1053-2005>, 2005.

628 Khalek, I. A., Bougher, T., and Jetter, J. J.: Particle Emissions from a 2009 gasoline direct injection
629 engine using different commercially available fuels, SAE Int. J. Fuels Lubr., 3(2), 623- 637,
630 <http://dio.org/10.4271/2010-01-2117>, 2010.

631 Kuwata, M., Liu, Y., McKinney, K., and Martin, S.T.: Physical state and acidity of inorganic sulfate
632 can regulate the production of secondary organic material from isoprene photooxidation
633 products, Phys Chem Chem Phys: PCCP, 17, 5670-5678, <http://dio.org/10.1039/C4CP04942J>,
634 2015.

635 Lack, D.A., Langridge, J.M., Bahreini, R., Cappa, C.D., Middlebrook, A.M., and Schwarz, J.P.:
636 Brown carbon and internal mixing in biomass burning particles, P Natl Acad Sci USA, 109,
637 <http://dio.org/14802-14807>, 10.1073/pnas.1206575109, 2012.

638 Lambe, A.T., Ahern, A.T., Wright, J.P., Croasdale, D.R., Davidovits, P., and Onasch, T.B.:
639 Oxidative aging and cloud condensation nuclei activation of laboratory combustion soot, J
640 Aerosol Sci, 79, 31-39, <http://dio.org/10.1016/j.jaerosci.2014.10.001>, 2015.

641 Lang-Yona, N., Abo-Riziq, A., Erlick, C., Segre, E., Trainic, M., and Rudich, Y.: Interaction of
642 internally mixed aerosols with light, Phys Chem Chem Phys, 12, 21-31,
643 <http://dio.org/10.1039/B913176K>, 2010.

644 Laskin, A., Laskin, J., and Nizkorodov, S.A.: Chemistry of Atmospheric Brown Carbon, Chem Rev,
645 115, 4335-4382, <http://dio.org/10.1021/cr5006167>, 2015.

646 Li, W., and Shao, L.: Transmission electron microscopy study of aerosol particles from the brown hazes
647 in northern china, J. Geophys. Res.-Atmos., <http://dio.org/D09302>, 2009.

648 Liati, A., Schreiber, D., Dasilva, Y. A. R., and Eggenchwiler, P. D.: Ultrafine particle emissions from
649 modern gasoline and diesel vehicles: An electron microscopic perspective, Environ. Pollut., 239,
650 661-669, <http://dio.org/10.1016/j.envpol.2018.04.081>, 2018.

651 Liu, L., Kong, S., Zhang, Y., Wang, Y., Xu, L., Yan, Q., Lingaswamy, A. P., Shi, Z., Lv, S., Niu, H.,
652 Shao, L., Hu, M., Zhang, D., Chen, J., Zhang, X., and Li, W.: Morphology, composition, and mixing
653 state of primary particles from combustion sources - crop residue, wood, and solid waste, Sci. Rep.-
654 UK, <http://dio.org/10.1038/s41598-017-05357-2>, 2017.

655 Loh, N.D., Hampton, C.Y., Martin, A.V., Starodub, D., Sierra, R.G., Barty, A., Aquila, A., Schulz,
656 J., Lomb, L., Steinbrener, J., Shoeman, R.L., Kassemeyer, S., Bostedt, C., Bozek, J., Epp, S.W.,
657 Erk, B., Hartmann, R., Rolles, D., Rudenko, A., Rudek, B., Foucar, L., Kimmel, N.,
658 Weidenspointner, G., Hauser, G., Holl, P., Pedersoli, E., Liang, M., Hunter, M.M., Gumprecht,
659 L., Coppola, N., Wunderer, C., Graafsma, H., Maia, F.R.N.C., Ekeberg, T., Hantke, M.,
660 Fleckenstein, H., Hirsemann, H., Nass, K., White, T.A., Tobias, H.J., Farquar, G.R., Benner,
661 W.H., Hau-Riege, S.P., Reich, C., Hartmann, A., Soltau, H., Marchesini, S., Bajt, S.,
662 Barthelmess, M., Bucksbaum, P., Hodgson, K.O., Strueder, L., Ullrich, J., Frank, M.,
663 Schlichting, I., Chapman, H.N., and Bogan, M.J.: Fractal morphology, imaging and mass
664 spectrometry of single aerosol particles in flight, *Nature*, 486, 513-517,
665 <http://dio.org/10.1038/nature11222>, 2012.

666 Lu, K.D., Hofzumahaus, A., Holland, F., Bohn, B., Brauers, T., Fuchs, H., Hu, M., H äseler, R., Kita,
667 K., Kondo, Y., Li, X., Lou, S.R., Oebel, A., Shao, M., Zeng, L.M., Wahner, A., Zhu, T., Zhang,
668 Y.H., and Rohrer, F.: Missing OH source in a suburban environment near Beijing: observed
669 and modelled OH and HO₂ concentrations in summer 2006, *Atmos Chem Phys*, 13, 1057-1080,
670 <http://dio.org/10.5194/acp-13-1057-2013>, 2013.

671 Luo, Y., Zhu, L., Fang, J., Zhuang, Z., Guan, C., Xia, C., Xie, X., and Huang, Z.: Size distribution,
672 chemical composition and oxidation reactivity of particulate matter from gasoline direct injection
673 (GDI) engine fueled with ethanol-gasoline fuel, *Appl. Therm. Eng.*, 89, 647-655,
674 <http://dio.org/10.1016/j.applthermaleng.2015.06.060>, 2015.

675 Ma, Q., Wu, Y., Zhang, D., Wang, X., Xia, Y., Liu, X., Tian, P., Han, Z., Xia, X., Wang, Y., and
676 Zhang, R.: Roles of regional transport and heterogeneous reactions in the PM_{2.5} increase during
677 winter haze episodes in Beijing, *Sci Total Environ*, 599, 246-253,
678 <http://dio.org/10.1016/j.scitotenv.2017.04.193>, 2017.

679 Maricq, M. M., Szente, J., Loos, M., and Vogt, R.: Motor vehicle PM emissions measurement at LEV
680 III levels, *SAE Int. J. Engines*, 4(1), 597- 609, <http://dio.org/10.4271/2011-01-0623>, 2011.

681 Mauldin, R. L. I., Berndt, T., Sipilae, M., Paasonen, P., Petaja, T., Kim, S., Kurten, T., Stratmann, F.,
682 Kerminen, V., and Kulmala, M.: A new atmospherically relevant oxidant of sulphur dioxide, *Nature*,
683 488(7410), 193-196, <http://dio.org/10.1038/nature11278>, 2012.

684 National Bureau of Statistics of China, 2018. China Statistical Yearbook 2018, part sixteen:
685 Transportation, post and telecommunications and software industry. Available on line at:
686 <http://www.stats.gov.cn/tjsj/ndsj/2018/indexch.htm>, 2018.

687 Niu, H., Cheng, W., Hu, W., and Pian, W.: Characteristics of individual particles in a severe short-period
688 haze episode induced by biomass burning in Beijing, *Atmos. Pollut. Res.*, 7(6), 1072-1081,
689 <http://dio.org/10.1016/j.apr.2016.05.011>, 2016.

690 Niu, H., Hu, W., Zhang, D., Wu, Z., and Guo, S.: Variations of fine particle physiochemical
691 properties during a heavy haze episode in the winter of Beijing, *Sci Total Environ*, 571, 103-
692 109, <http://dio.org/10.1016/j.scitotenv.2016.07.147>, 2016.

693 Niu, H., Shao, L., and Zhang, D.: Aged status of soot particles during the passage of a weak cyclone in
694 Beijing, *Atmos. Environ.*, 45(16), 2699-2703, <http://dio.org/10.1016/j.atmosenv.2011.02.056>, 2011.

695 Okada, K., Qin, Y., and Kai, K.: Elemental composition and mixing properties of atmospheric mineral
696 particles collected in Hohhot, China, *Atmos. Res.*, 73(1-2), 45-67,
697 <http://dio.org/10.1016/j.atmosres.2004.08.001>, 2005.

698 Peng, J., Hu, M., Guo, S., Du, Z., Shang, D., Zheng, J., Zheng, J., Zeng, L., Shao, M., Wu, Y., Collins,

699 D., and Zhang, R.: Ageing and hygroscopicity variation of black carbon particles in Beijing
700 measured by a quasi-atmospheric aerosol evolution study (QUALITY) chamber, *Atmos. Chem.*
701 *Phys.*, 17(17), 10333-10348, <http://dio.org/10.5194/acp-17-10333-2017>, 2017.

702 Peng, J.F., Hu, M., Wang, Z.B., Huang, X.F., Kumar, P., Wu, Z.J., Guo, S., Yue, D.L., Shang, D.J.,
703 Zheng, Z., and He, L.Y.: Submicron aerosols at thirteen diversified sites in China: size distribution,
704 new particle formation and corresponding contribution to cloud condensation nuclei production,
705 *Atmos Chem Phys*, 14, 10249-10265, [10.5194/acp-14-10249-2014](http://dio.org/10.5194/acp-14-10249-2014), 2014.

706 Petzold, A., Marsh, R., Johnson, M., Miller, M., Sevcenco, Y., Delhaye, D., Ibrahim, A., Williams, P.,
707 Bauer, H., Crayford, A., Bachalo, W. D., and Raper, D.: Evaluation of methods for measuring
708 particulate matter emissions from gas turbines, *Environ. Sci. Technol.*, 45(8), 3562-3568, 2011.

709 Rönkkö, T., Löhde, T., Heikkilä, J., Pirjola, L., Bauschke, U., Arnold, F., Schlager, H., Rothe, D., Yli-
710 Ojanperä, J., and Keskinen, J.: Effects of gaseous sulphuric acid on diesel exhaust nanoparticle
711 formation and characteristics, *Environ. Sci. Technol.*, 47(20), 11882-11889,
712 <http://dio.org/10.1021/es402354y>, 2013.

713 Scott, C. E., Rap, A., Spracklen, D. V., Forster, P. M., Carslaw, K. S., Mann, G. W., Pringle, K. J.,
714 Kivekas, N., Kulmala, M., Lihavainen, H., and Tunved, P.: The direct and indirect radiative effects
715 of biogenic secondary organic aerosol, *Atmos. Chem. Phys.*, 14(1), 447-470,
716 <http://dio.org/10.5194/acp-14-447-2014>, 2014.

717 Shao, L., Hu, Y., Fan, J., Wang, J., Wang, J., and Ma, J.: Physicochemical characteristics of aerosol
718 particles in the Tibetan Plateau: Insights from TEM-EDX analysis, *J. Nanosci. Nanotechnol.*, 17(9),
719 6899-6908, <http://dio.org/10.1166/jnn.2017.14472>, 2017.

720 Shao, L., Hu, Y., Shen, R., Schäfer, K., Wang, J., Wang, J., Schnelle-Kreis, J., Zimmermann, R., Bérubé
721 K., and Suppan, P.: Seasonal variation of particle-induced oxidative potential of airborne particulate
722 matter in Beijing, *Sci. Total Environ.*, 579, 1152-1160,
723 <http://dio.org/10.1016/j.scitotenv.2016.11.094>, 2017.

724 Song, C., Na, K., Warren, B., Malloy, Q., and Cocker, D.R.: Secondary Organic Aerosol Formation from
725 m-Xylene in the Absence of NO_x, *Environ Sci Technol*, 41, 7409-7416,
726 <http://dio.org/10.1021/es070429r>, 2007.

727 Song, M., Zhang, C., Wu, H., Mu, Y., Ma, Z., Zhang, Y., Liu, J., and Li, X.: The influence of OH
728 concentration on SOA formation from isoprene photooxidation, *Sci Total Environ*, 650, 951-957,
729 <http://dio.org/10.1016/j.scitotenv.2018.09.084>, 2019.

730 Shi, Z., Vu, T., Kotthaus, S., Harrison, R. M., Grimmond, S., Yue, S., Zhu, T., Lee, J., Han, Y., Demuzere,
731 M., Dunmore, R. E., Ren, L., Liu, D., Wang, Y., Wild, O., Allan, J., Acton, W. J., Barlow, J., Barratt,
732 B., Beddows, D., Bloss, W. J., Calzolari, G., Carruthers, D., Carslaw, D. C., Chan, Q., Chatzidiakou,
733 L., Chen, Y., Crilley, L., Coe, H., Dai, T., Doherty, R., Duan, F., Fu, P., Ge, B., Ge, M., Guan, D.,
734 Hamilton, J. F., He, K., Heal, M., Heard, D., Hewitt, C. N., Hollaway, M., Hu, M., Ji, D., Jiang, X.,
735 Jones, R., Kalberer, M., Kelly, F. J., Kramer, L., Langford, B., Lin, C., Lewis, A. C., Li, J., Li, W.,
736 Liu, H., Liu, J., Loh, M., Lu, K., Lucarelli, F., Mann, G., McFiggans, G., Miller, M. R., Mills, G.,
737 Monk, P., Nemitz, E., O'Connor, F., Ouyang, B., Palmer, P. I., Percival, C., Popoola, O., Reeves,
738 C., Rickard, A. R., Shao, L., Shi, G., Spracklen, D., Stevenson, D., Sun, Y., Sun, Z., Tao, S., Tong,
739 S., Wang, Q., Wang, W., Wang, X., Wang, X., Wang, Z., Wei, L., Whalley, L., Wu, X., Wu, Z.,
740 Xie, P., Yang, F., Zhang, Q., Zhang, Y., Zhang, Y., and Zheng, M.: Introduction to the special issue
741 "In-depth study of air pollution sources and processes within Beijing and its surrounding region
742 (APHH-Beijing)", *Atmos. Chem. Phys.*, 19(11), 7519-7546, <http://dio.org/10.5194/acp-19-7519->

743 2019, 2019.

744 Suarez-Bertoa, R., Zardini, A. A., Platt, S. M., Hellebust, S., Pieber, S. M., El Haddad, I., Temime-
745 Roussel, B., Baltensperger, U., Marchand, N., Prévôt, A. S. H., and Astorga, C.: Primary emissions
746 and secondary organic aerosol formation from the exhaust of a flex-fuel (ethanol) vehicle, *Atmos.*
747 *Environ.*, 117, 200-211, <http://dio.org/10.1016/j.atmosenv.2015.07.006>, 2015.

748 Szybist, J. P., Youngquist, A. D., Barone, T. L., Storey, J. M., and Moore, W. R.: Ethanol blends and
749 engine operating strategy effects on light-duty spark-ignition engine particle emissions, *Energ. Fuel.*,
750 25(11), 4977-4985, <http://dio.org/10.1021/ef201127y>, 2011.

751 Wang, W., Shao, L., Li, J., Chang, L., Zhang, D., Zhang, C., and Jiang, J.: Characteristics of individual
752 particles emitted from an experimental burning chamber with coal from the lung cancer area of
753 Xuanwei, China, *Aerosol Air Qual. Res.*, 19(2), 355-363, <http://dio.org/10.4209/aaqr.2018.05.0187>,
754 2019.

755 Xing, J., Shao, L., Zhang, W., Peng, J., Wang, W., Hou, C., Shuai, S., Hu, M., and Zhang, D.:
756 Morphology and composition of particles emitted from a port fuel injection gasoline vehicle under
757 real-world driving test cycles, *J. Environ. Sci-China*, 76, 339-348,
758 <http://dio.org/10.1016/j.jes.2018.05.026>, 2019.

759 Xing, J., Shao, L., Zheng, R., Peng, J., Wang, W., Guo, Q., Wang, Y., Qin, Y., Shuai, S., and Hu, M.:
760 Individual particles emitted from gasoline engines: Impact of engine types, engine loads and fuel
761 components, *J. Clean. Prod.*, 149, 461-471, <http://dio.org/10.1016/j.jclepro.2017.02.056>, 2017.

762 Yu, L., Wang, G., Zhang, R., Zhang, L., Song, Y., Wu, B., Li, X., An, K., and Chu, J.: Characterization
763 and source apportionment of PM_{2.5} in an urban environment in Beijing, *Aerosol Air Qual. Res.*,
764 13(2), 574-583, 2013.

765 Zhang, H., Cheng, S., Li, J., Yao, S., and Wang, X.: Investigating the aerosol mass and chemical
766 components characteristics and feedback effects on the meteorological factors in the
767 Beijing-Tianjin-Hebei region, China, *Environ. Pollut.*, 244, 495-502,
768 <http://dio.org/10.1016/j.envpol.2018.10.087>, 2019.

769 Zhang, M., Li, Z., Xu, M., Yue, J., Cai, Z., Yung, K.K.L., and Li, R.: Pollution characteristics,
770 source apportionment and health risks assessment of fine particulate matter during a
771 typical winter and summer time period in urban Taiyuan, China, *Hum Ecol Risk Assess.*,
772 <http://dio.org/10.1080/10807039.2019.1684184>, 2019.

773 Zhang, Y., Yuan, Q., Huang, D., Kong, S., Zhang, J., Wang, X., Lu, C., Shi, Z., Zhang, X., Sun, Y.,
774 Wang, Z., Shao, L., Zhu, J., and Li, W.: Direct observations of fine primary particles from residential
775 coal burning: Insights into their morphology, composition, and hygroscopicity, *J. Geophys. Res.-*
776 *Atmos.*, 123(22), 12,964-12,979, <http://dio.org/10.1029/2018JD028988>, 2018.

777 Zhu, J., Penner, J. E., Lin, G., Zhou, C., Xu, L., and Zhuang, B.: Mechanism of SOA formation
778 determines magnitude of radiative effects, *P. Natl. Acad. Sci. USA*, 114(48), 12685-12690,
779 <http://dio.org/10.1073/pnas.1712273114>, 2017.

780 Zimmerman, N., Wang, J. M., Jeong, C., Ramos, M., Hilker, N., Healy, R. M., Sabaliauskas, K., Wallace,
781 J. S., and Evans, G. J.: Field measurements of gasoline direct injection emission factors: Spatial and
782 seasonal variability, *Environ. Sci. Technol.*, 50(4), 2035-2043,
783 <http://dio.org/10.1021/acs.est.5b04444>, 2016.

784

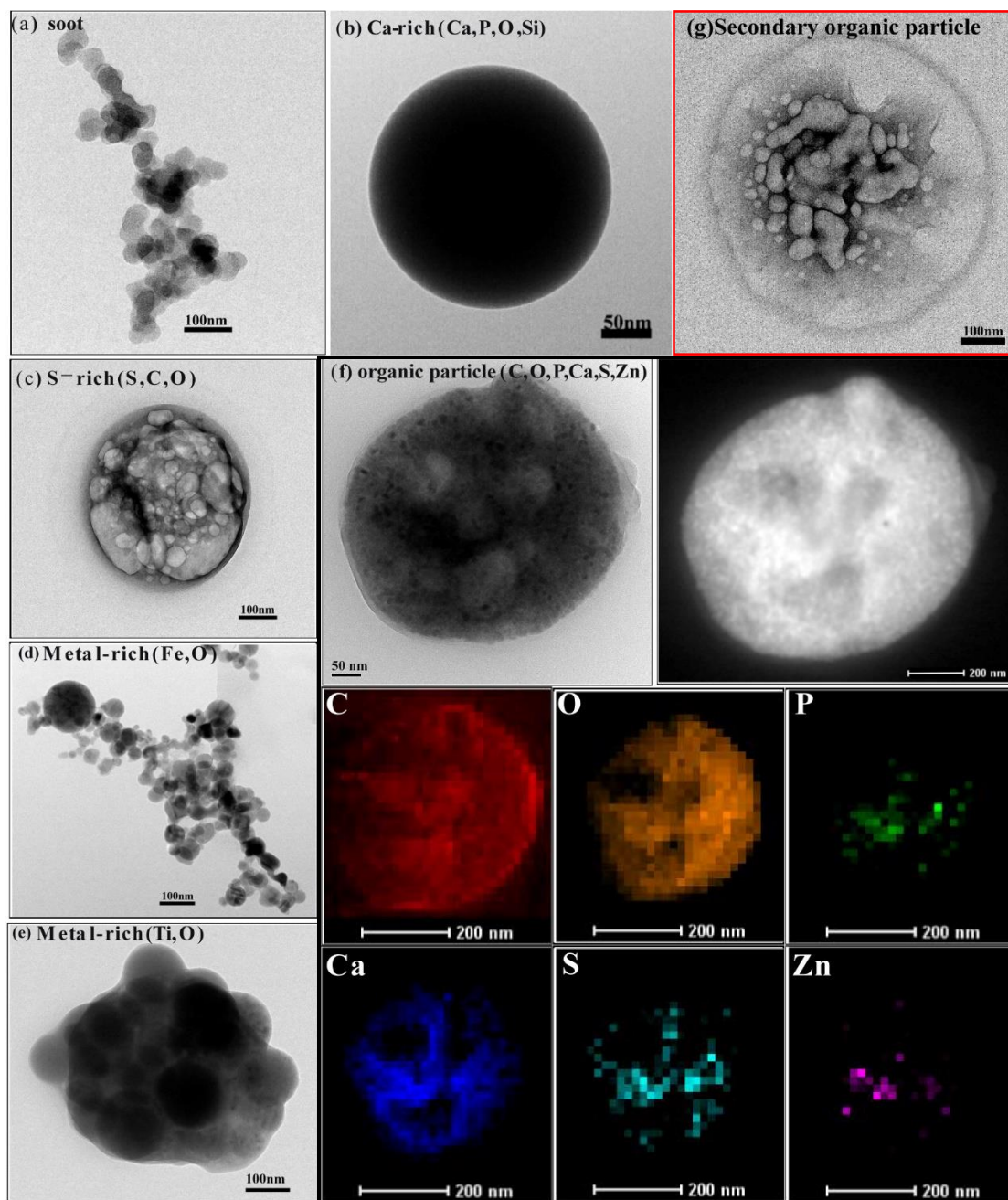
785 **List of tables:**786 Table 1 Comparison of chemical components between various sources including fossil
787 fuels, biomass burning and urban waste burning

| Study | Source | Particle of type and relative percentages | Chemical composition of organic particles |
|---------------------|------------------------------|--|---|
| This study | GDI-engine vehicles | Organic particles (OM) (32%), Soot (32%), Ca-rich particles (26%), S-rich (5%) and metal-containing particles (4%) | OM with Ca and weak P, S, and Zn |
| Xing et al. (2019) | PFI-engine vehicles | OM (44%), soot (23%), Ca-rich particles (20%), S-rich (6%) and metal-containing particles (6%). | OM with Ca and weak P, S, and Zn. |
| Liati et al. (2018) | GDI, PFI and diesel vehicles | Soot, OM (called ash-bearing soot particles) and ash particles. | OM with Ca, S, P, Fe and minor Zn. |
| Liu et al. (2017) | Crop residue combustion | OM (27%), OM-K (43%), OM-soot-K (27%), soot-OM (3%). | OM particles with K content. |
| Liu et al. (2017) | Wood combustion | OM (16%), soot (18%), OM-K (22%), OM-soot-K (15%), soot-OM (29%). | OM particles with K content. |
| Wang et al. (2019) | Coal burning | OM (38%), soot (40%), S-rich particles (2%), and mineral particles (18%). | OM mainly consisted of C, O and Si. |
| Zhang et al. (2018) | Residential coal burning | OM (51%), OM-S (24%), soot-OM (23%), S-rich (1%), metal-rich particles (1%), mineral particles (1%). | OM contained C, O, and Si with minor amounts of S and Cl. |

788

789

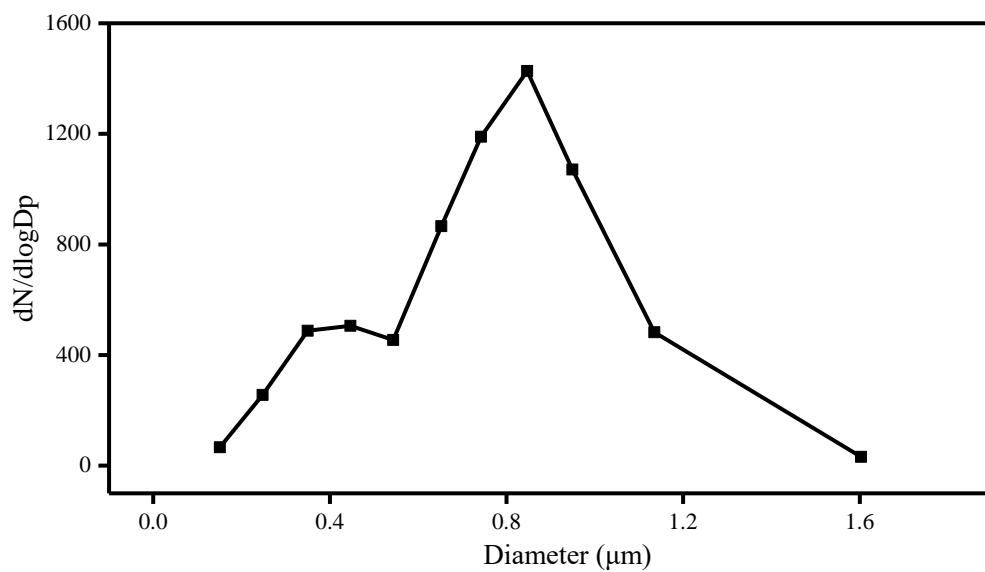
790 **List of figures:**



791

792 Figure 1. TEM images of the individual primary particles emitted from the GDI-engine
793 gasoline vehicle and the secondary organic particle in the chamber after exposure to
794 ambient sunlight for 3.5 hours. (a) soot particle; (b) Ca-rich particle; (c) S-rich particles;
795 (d) Metal-rich particles (Fe); (e) Metal-rich particles (Ti); (f) bright-field-TEM and
796 dark-field-TEM image of organic particles, and others are the mapping of the C, O, P,
797 Ca, S, and Zn in the organic particle; (g) secondary organic particle in chamber.

798



799

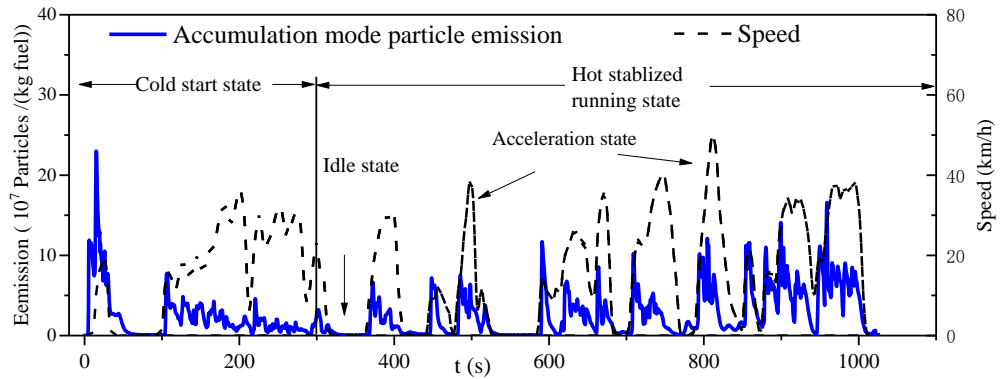
800 Figure 2. Size distribution of analyzed particles emitted from the GDI-engine gasoline
801 vehicles by the TEM images. In total, 2880 particles were analyzed from the GDI-
802 engine vehicles. Particles smaller than 0.25 µm should have been underestimated
803 because of the collection efficiency of the impactor.

804

805

806

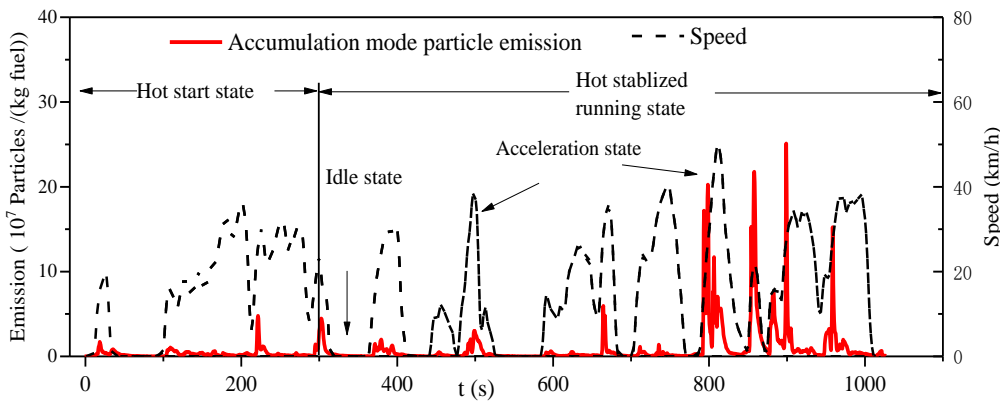
(a)



807

808

(b)

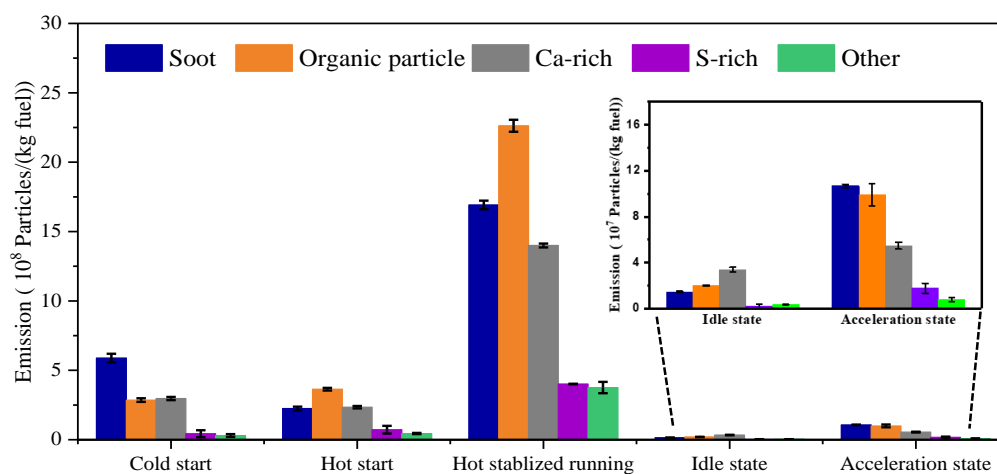


809

810 Figure 3. Particles in accumulation mode from the GDI vehicle during cold start (a) and
811 hot start (b) driving cycle. The vehicle speed is also shown for reference. Before the
812 test with cold start, the temperatures of the engine coolant and oil could not differ by
813 more than 2 °C during the soak temperature. The hot start test was conducted within 5
814 mins after the cold start test. The number concentration of particles during the tests was
815 monitored by DMS 500.

816

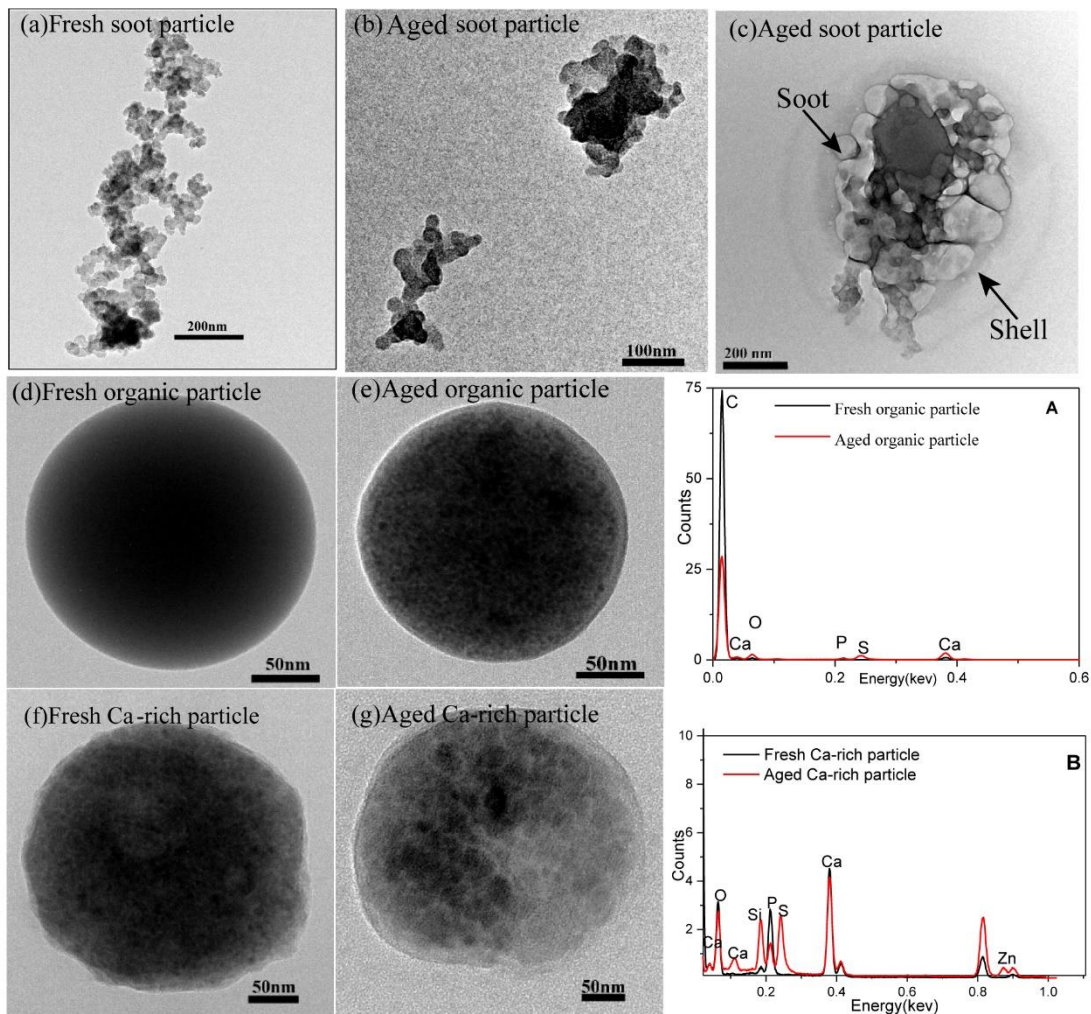
817



819

820 Figure 4. The number of different type particles in the emissions from the GDI vehicle
 821 under the different running states by the burning of per unit of fuel, including cold start,
 822 hot start, hot stabilization, idle, and acceleration states. Data presented as
 823 mean \pm standard deviation, N = 3.

824



825

826 Figure 5. TEM images of particles in the chamber after exposure to ambient sunlight
 827 for 3.5 hours. (a) Fresh soot particles; (b) Aged soot particles; (c) Aged soot particle (d)
 828 Fresh organic particle (e) Aged organic particle (f) Fresh Ca-rich particle (g) Aged Ca-
 829 rich particle (A) EDX spectrum for a fresh organic particle and an aged organic particle.
 830 (B) EDX spectrum for a fresh organic particle and an aged Ca-rich particle.